Reggeometry of deeply virtual Compton scattering and exclusive diffractive vector meson production at HERA

S. Fazio[a*], R. Fiore[b‡], L. Jenkovszky[c,d†], A. Lavorini[b⋆], and A. Saliy[c ⋄]

[a] *Brookhaven National Laboratory, Physics Department*
11973 Upton, NY - U.S.A.

[b] *Dipartimento di Fisica, Universitá della Calabria*
Istituto Nazionale di Fisica Nucleare, Gruppo collegato di Cosenza
I-87036 Arcavacata di Rende, Cosenza, Italy

[c] *Bogolyubov Institute for Theoretical Physics,*
National Academy of Sciences of Ukraine
UA-03680 Kiev, Ukraine

[d] *Wigner Research Centre for Physics, Hungarian Academy of Sciences*
1525 Budapest, POB 49, Hungary

Regge-pole models do not know about the t and Q^2, M_V dependence of the scattering amplitude. We extend a simple Pomeron pole amplitude by t and Q^2, M_V dependencies inspired by geometrical ideas. The experimentally transition from *soft* to *hard* dynamics is realized by the introduction of two Pomeron poles with different Q^2 M_V- dependent residue. A unified description of deeply virtual Compton scattering as well as the elastic electroproduction of all vector meson is suggested.

*e-mail address: sfazio@bnl.gov
‡e-mail address: fiore@cs.infn.it
†e-mail address: jenk@bitp.kiev.ua
⋆e-mail address: aadelmo.lavorini@gmail.com
⋄e-mail address: saliy.andriy@gmail.com

1 Introduction

The forward slope of the the differential cross sections for elastic scattering is known to be related to the masses/virtualities of the interacting particles. This phenomenon is evident e.g. from Fig. (SLOPES), where the forward slope $B(\tilde{Q}^2) = \frac{d}{dt} \ln \frac{d\sigma}{dt}$ is plotted against the the variable $\tilde{Q}^2 = Q^2 + M_V^2$ [a]. The slope, proportional to the *interaction radius* $R(\tilde{Q}^2)$, decreases with increasing $\tilde{Q}^2$, reaching some saturation value, determined by the finite mass of the nucleons. In this *geometric* picture, the largest slope (radius) is expected for real Compton scattering $\tilde{Q}^2 = 0$, which may require a separate treatment.

[a] The use of the variable $\tilde{Q}^2 = (M_V^2 + Q^2)$ implies symmetry between the mass M_V^2 and virturality Q^2, which should imply equal slopes (radii) for e.g. J/ψ production near $Q^2 = 0$ and ρ electroproduction near $Q^2 \approx 9$ GeV^2, which is not supported by the data.

In the present paper we consider exclusive diffractive electroproduction of real photons and vector mesons as well as elastic proton-proton scattering by making use of the above *geometric* considerations, by writing the scattering amplitude in the form:

$$A(s,t) \sim e^{B(s,M_V^2)t} \tag{1}$$

with $B(M^2) \sim 1/f(M_V^2)$. This approach was used in Ref. [2] for the simpler case of photoproduction, $\tilde{Q}^2 = 0$, excluding real Compton scattering, and without considering nucleon scattering, to be also included below.
While the geometric considerations proved to be efficient [2] for photoproduction, they are not sufficient in the case of electroproduction $Q^2 = 0$, since the relevant cross sections will increase with $\tilde{Q}^2$ contradicting the experimental data. To remedy this deficiency, this rise must be compensated by multiplying the amplitude by a function decreasing with $\tilde{Q}^2$. Moreover, to cope with the observed trend of *hardening* the dynamics as $\tilde{Q}^2$ increases, and following Refs. [5,6], we introduce two components for the diffractive (Pomeron) amplitude of the type Eq. (1), soft A_s and hard A_h, each one to be multiplied by a relevant $\tilde{Q}^2-$dependent factor $H_i(\tilde{Q}^2),\ i = s, h$. These factors are chosen in such a way as provide for the increasing weight of the hard component as the mass (virtuality) increases. To avoid conflict with unitarity, the rise with $\tilde{Q}^2$ of the hard component is finite, and it terminates at some *saturation* scale $\tilde{Q}_0^2$ whose value is determined phenomenologically. Explicit examples of these functions will be given below.

Recently [1,4] a model for exclusive production of vector particles at HERA was suggested and successfully fitted to the HERA data. In that model, the interplay between t and $\tilde{Q}^2$ is achieved by introducing a new variable $z = t - \tilde{Q}^2$. Good fits were obtained at those papers, however the specific interplay between the variables t and Q^2 there awaits for a better understanding and physical inerpretation.

2 The Model

2.1 Regge+geometry=Reggeometry

Quite generally, the Regge-pole scattering amplitude can be written as

$$A(s,t,M,Q^2) = \xi(t)\beta(t,M,Q^2)(s/s_0)^{\alpha(t)}, \tag{2}$$

where $\xi(t) = e^{-i\pi\alpha(t)}$ is the signature factor and $\beta(t,M,Q^2)$ is the residue factor written in the following geometrical form:

$$\beta(t,M,Q^2) = \exp\Big[4\Big(\frac{a}{M_V^2+Q^2} + \frac{b}{2m_N^2}\Big)t\Big]. \tag{3}$$

Hence

$$A(s,t,M,Q^2) = \tilde{A}_0\xi(t)(s/s_0)^{\alpha(t)}e^{-4\left(\frac{a}{M_V^2+Q^2}+\frac{b}{2m_N^2}\right)|t|}. \tag{4}$$

The differential cross section is

$$\frac{d\sigma}{d|t|} = \frac{\pi}{s^2}|A(s,t,M,Q^2)|^2 = A_0(s/s_0)^{2(\alpha_0-1-\alpha'|t|)}e^{-8\left(\frac{a}{M_V^2+Q^2}+\frac{b}{2m_N^2}\right)|t|}, \tag{5}$$

or

$$\frac{d\sigma}{d|t|} = A_0(s/s_0)^{2(\alpha_0-1)}e^{-\left[2\alpha'\ln(s/s_0)+8\left(\frac{a}{M_V^2+Q^2}+\frac{b}{2m_N^2}\right)\right]|t|} = Ce^{-B|t|}. \tag{6}$$

The local slope paremeter is defined as

$$B(s,\tilde{Q}^2)=\frac{d}{dt}\ln\frac{d\sigma}{d|t|}=2\alpha'\ln(s/s_0)+8\Big(\frac{a}{M_V^2+Q^2}+\frac{b}{2m_N^2}\Big), \tag{7}$$

and the integrated elastic scattering amplitude is

$$\sigma_{el}=\frac{1}{B}\frac{d\sigma}{dt}\Big|_{t=0}=\frac{C}{B}, \tag{8}$$

or

$$\sigma_{el}=\frac{A_0(s/s_0)^{2(\alpha_0-1)}}{2\alpha'\ln(s/s_0)+8\Big(\frac{a}{M_V^2+Q^2}+\frac{b}{2m_N^2}\Big)}. \tag{9}$$

In the case $a>0$ when $\tilde{Q}^2=M_V^2+Q^2$ grows, $B(s,\tilde{Q}^2)$ falls, but $\frac{d\sigma}{d|t|}$ and σ_{el} become larger. While the behavior of $B(s,\tilde{Q}^2)$ is conistent with the experimental data, the behavior of $\frac{d\sigma}{d|t|}$ and σ_{el} are not.

2.2 Soft and Hard components of the unique Pomeron

We build the scattering amplitude that contain two terms, soft and hard, with two different $\widetilde{Q^2}$-dependent factors:

$$A(s,t,Q^2,{M_V}^2)=\frac{\tilde{A}_s}{\Big(1+\frac{\widetilde{Q^2}}{\widetilde{Q_s^2}}\Big)^{n_s}}e^{-i\frac{\pi}{2}\alpha_s(t)}\Big(\frac{s}{s_{0s}}\Big)^{\alpha_s(t)}e^{2\Big(\frac{a_s}{\widetilde{Q^2}}+\frac{b_s}{2m_p^2}\Big)t} \tag{10}$$

$$+\frac{\tilde{A}_h\Big(\frac{\widetilde{Q^2}}{\widetilde{Q_h^2}}\Big)}{\Big(1+\frac{\widetilde{Q^2}}{\widetilde{Q_h^2}}\Big)^{n_h+1}}e^{-i\frac{\pi}{2}\alpha_h(t)}\Big(\frac{s}{s_{0h}}\Big)^{\alpha_h(t)}e^{2\Big(\frac{a_h}{\widetilde{Q^2}}+\frac{b_h}{2m_p^2}\Big)t}.$$

The $\tilde{Q}^2-$ dependent factors were introduced in such a way as to provide for a proper balance between the soft and hard components of the Pomeron, namely that the hard one increases with increasing $\tilde{Q}^2$, up to the saturation point, thus securing unitarity. The extra $\tilde{Q}^2-$dependent (but $t-$ independent!) factor does not violate the geometrical structure of the amplitude.

The differential and integrated cross sections now are:

$$\frac{d\sigma_{el}}{d|t|}=H_s^2e^{2\{L_s(\alpha_s(t)-1)+\mathfrak{g}_\mathfrak{s}t\}}+H_h^2e^{2\{L_h(\alpha_h(t)-1)+\mathfrak{g}_\mathfrak{h}t\}} \tag{11}$$

$$+2H_sH_he^{\{L_s(\alpha_s(t)-1)+L_h(\alpha_h(t)-1)+(\mathfrak{g}_\mathfrak{s}+\mathfrak{g}_\mathfrak{h})t\}}\cos\Big(\frac{\pi}{2}(\alpha_s(t)-\alpha_h(t))\Big),$$

$$\sigma_{el}=\frac{H_s^2e^{2\{L_s(\alpha_{0s}-1)\}}}{2(\alpha_s'L_s+\mathfrak{g}_\mathfrak{s})}+\frac{H_h^2e^{2\{L_h(\alpha_{0h}-1)\}}}{2(\alpha_h'L_h+\mathfrak{g}_\mathfrak{h})}+2H_sH_he^{L_s(\alpha_{0s}-1)+L_h(\alpha_{0h}-1)}\frac{\mathfrak{B}\cos\phi_0+\mathfrak{L}\sin\phi_0}{\mathfrak{B}^2+\mathfrak{L}^2}, \tag{12}$$

where the notation $H_s=\frac{A_s}{\Big(1+\frac{\widetilde{Q^2}}{\widetilde{Q_s^2}}\Big)^{n_s}}$, $\quad H_h=\frac{A_h\Big(\frac{\widetilde{Q^2}}{Q_h^2}\Big)}{\Big(1+\frac{\widetilde{Q^2}}{\widetilde{Q_h^2}}\Big)^{n_h+1}}$,

$L_s = \ln\left(\frac{s}{s_{0s}}\right), \quad \mathfrak{g}_{\mathfrak{s}} = 2\left(\frac{a_s}{\widetilde{Q^2}} + \frac{b_s}{2m_p^2}\right), \qquad \alpha_s(t) = \alpha_{0s} + \alpha'_s t,$

$L_h = \ln\left(\frac{s}{s_{0h}}\right), \quad \mathfrak{g}_{\mathfrak{h}} = 2\left(\frac{a_h}{\widetilde{Q^2}} + \frac{b_h}{2m_p^2}\right),, \quad \alpha_h(t) = \alpha_{0h} + \alpha'_h t,$

$\mathfrak{B} = L_s\alpha'_s + L_h\alpha'_h + (\mathfrak{g}_{\mathfrak{s}} + \mathfrak{g}_{\mathfrak{h}}),$

$\mathfrak{L} = \frac{\pi}{2}(\alpha'_s - \alpha'_h),$

$\phi_0 = \frac{\pi}{2}(\alpha_{0s} - \alpha_{0h})$

was introduced.

For the soft and hard components of the Pomeron trajectory we use the Donnachie-Landshoff parameterization [5,6]:

$$DL \quad pomerons: \quad \begin{array}{l} \alpha_s(t) = 1.08 + 0.25t, \\ \alpha_h(t) = 1.44 + 0.01t. \end{array}$$

3 Fits to the data

Although there are 16 fitting parameters, almost all of them can be fixed.

$$\left(\begin{array}{cccccccc} & & fix, & fix, & fix, & fix, & fix, & fix \\ A_s, & \widetilde{Q_s^2}, & n_s, & s_{0s}, & \alpha_{0s}, & \alpha'_s, & a_s, & b_s \\ A_h, & \widetilde{Q_h^2}, & n_h, & s_{0h}, & \alpha_{0h}, & \alpha'_h, & a_h, & b_h \end{array} \right)$$

The values of the parameters obtained form fitting the DVCS differential elastic cross section are:

	A_s	$\widetilde{Q_s^2}$	n_s	s_{0s}	α_{0s}	α'_s	a_s	b_s
$soft:$	$3.437 \pm 3.587;$	$23.724 \pm 36.520;$	2;	7.0;	1.08;	0.25;	1.0;	1.0;
$hard:$	$2.466 \pm 27.216;$	$1.535 \pm 7.243;$	2;	7.0;	1.44;	0.01;	1.0;	1.0;

and those form fitting the integrated elastic DVCS cross section are:

	A_s	$\widetilde{Q_s^2}$	n_s	s_{0s}	α_{0s}	α'_s	a_s	b_s
$soft:$	$2.448 \pm 2.118;$	$29.683 \pm 38.633;$	2;	7.0;	1.08;	0.25;	1.0;	1.0;
$hard:$	$2.458 \pm 2.744;$	$1.705 \pm 2.089;$	2;	7.0;	1.44;	0.01;	1.0;	1.0;

These two fits were performed separately, giving similar results. The experimental data for the fits are from Refs. [7,8,9,10].

The results of the fit are shown in the figures appended.

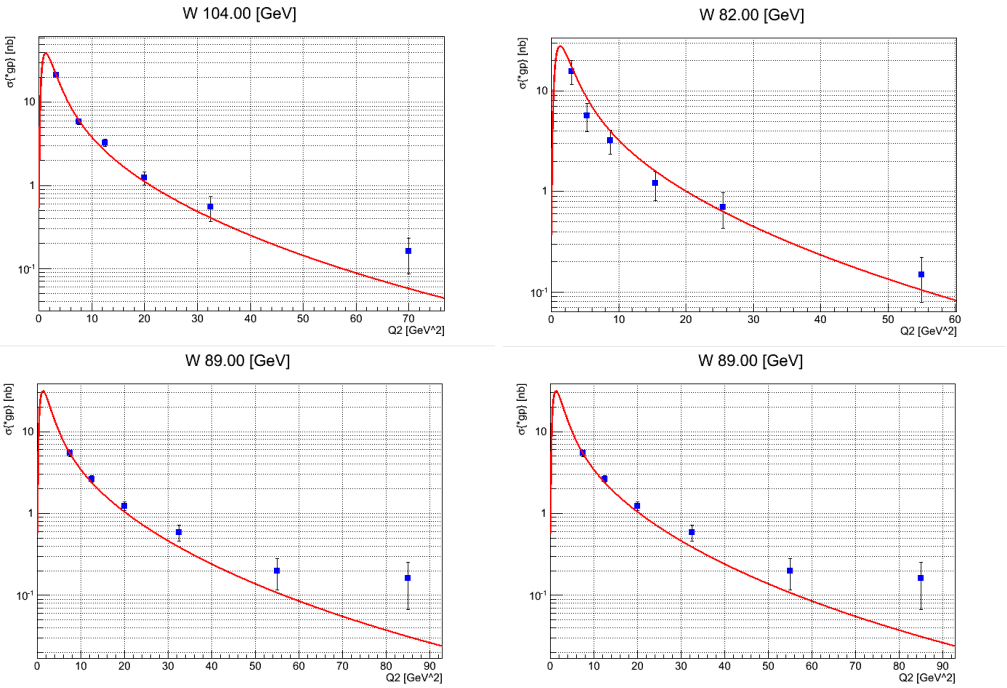

Figure 1: Results of our fit to $\gamma^* p \rightarrow \gamma p$ elastic cross-section as a function of Q^2 for ZEUS 99-00 (upper, left icon) and H1 96-00 (upper, right icon); for ZEUS 96-00 (lower left and right icons).

Acknowledgments

L.J. thanks the Department of Physics of the University of Calabria and the Istituto Nazionale di Fisica Nucleare - Sezione di Torino and Gruppo Collegato di Cosenza, where part of this work was done, for their hospitality and support.

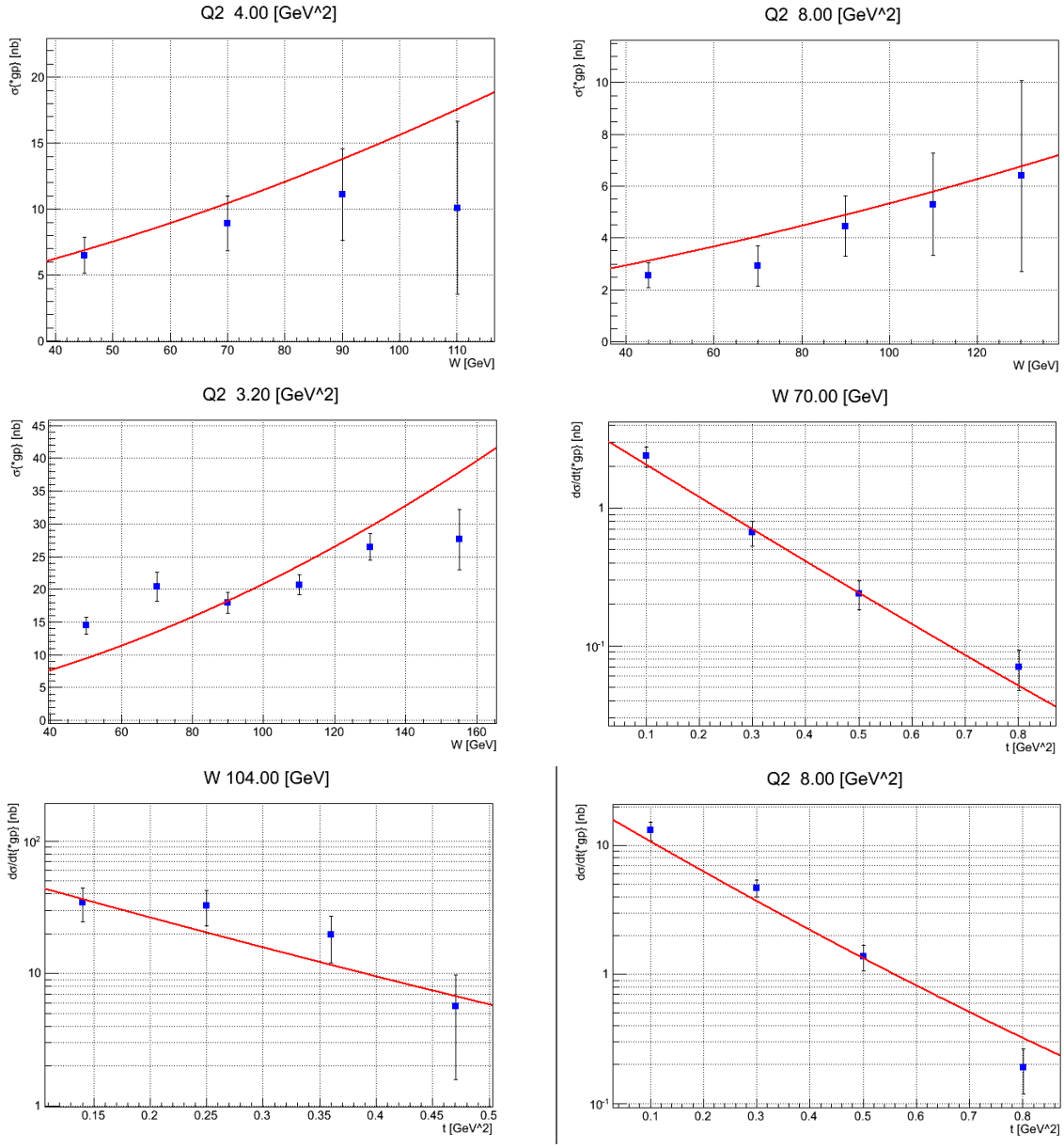

Figure 2: Results of our fit to $\gamma^* p \rightarrow \gamma p$ elastic cross-section as a function of W for ZEUS 99-00 (upper left and middle left icons) and H1 05-06 (upper right, icon); $\gamma^* p \rightarrow \gamma p$ differential cross-section as a function of t for ZEUS 99-00 (down-left) and H1 05-06 (middle and lower, right icons).

References

1. M. Capua, S. Fazio, R. Fiore, L. Jenkovszky, F. Paccanoni, Phys. Letters B **645**, 161 (2007) 161; hep-ph/0605319.
2. R.Fiore, L.L. Jenkovszky and F. Paccanoni, arXiv:hep-ph/9812458 [pdf, ps, other] *Photoproduction of Heavy Vector Mesons at HERA – A Testfield for Diffraction*, Eur. Phys. J. **C10** (1999) 461-467; hep-ph/9812458.
3. M. Capua, R. Fiore, S. Fazio, L. Jenkovszky, and F. Paccanoni, Phys. Lett. B **645** (2007) 161; hep-ph/0605319.
4. S. Fazio, R. Fiore, L.L. Jenkovszky and A.A. Lavorini, Phys. Rev. **C 85**, 5 (2012); hep-ph/1109.6374.
5. P. Landshoff, hep-ph/0903.1523.
6. A. Donnachie, P.V. Landshoff, hep-ph/0803.0686.
7. H1 Coll., A. Atkas et al., Eur. Phys. J. **C 44**, 1 (2005).
8. H1 Coll., F.D. Aaron et al., Phys. Lett. **B 659**, 796 (2008).
9. H1 Coll., F. D. Aaron et al., Phys. Lett. **B 681**, 391 (2009).
10. ZEUS Coll., S. Chekanov et al., JHEP **0905**, 108 (2009).